IEEE/CSC & ESAS European Superconductivity News Forum (ESNF), No. 6, October 2008
(ASC Preprint 2LPV06 conforming to IEEE Policy on Electronic Dissemination, Section 8.1.9)
The published version of this manuscript appeared in *IEEE Transactions on Applied Superconductivity* **19**, No. 3, Part 2, 1669-1673 (2009)

Proposal of a Fully Superconducting Motor for Liquid Hydrogen Pump With MgB_2 Wire

Kazuhiro Kajikawa and Taketsune Nakamura

***Abstract*—The outline design of a fully superconducting motor for liquid hydrogen pump with a magnesium-diboride (MgB_2) superconducting wire is carried out to present various advantages arising from its prospective performances. The squirrel-cage rotor winding composed of superconducting loops with the MgB_2 wire enables us to operate the motor not only in a slip mode but also in a synchronous rotation mode, and consequently the rotor winding loss can be suppressed drastically. Furthermore, it would be expected that the stator winding loss becomes smaller by using the MgB_2 wire compared with familiar normal metals as typified by a copper. The time evolution of magnetic field distribution around the stator winding is obtained by means of a finite element analysis in order to estimate the AC loss and the primary circuit resistance.**

***Index Terms*—Liquid hydrogen, magnesium diboride, superconducting motor, transfer line.**

I. Introduction

POSSIBILITIES of the future society with hydrogen utilization have been discussed as one of the advanced technologies for improvement of energy and environmental problems in recent decades [1]. In order to obtain effective energies by oxidizing the hydrogen with a fuel cell etc., it is necessary to produce, transport, store, and transfer the hydrogen safely and stably. In such situations, it can also be essential to use the hydrogen as a liquefied gas as well as a compressed gas. This is because the mass density of the compressed gaseous hydrogen is smaller than that for the hydrogen in the liquid phase as shown in Table I [2], and therefore the storage with the liquid hydrogen seems to be more compact and efficient. On the other hand, the slush hydrogen, a mixture of solid and liquid hydrogen, offers advantages of higher density (16%) and higher heat capacity (18%) than the liquid hydrogen [3].

The magnesium diboride (MgB_2) that is a new metallic superconductor discovered in the beginning of the 21st century has the transition temperature of 39 K [4], this material can keep a superconducting state with zero resistivity in the liquid hydrogen temperature. Since the critical current density at 20 K in the present wires composed of the MgB_2 superconductor decreases markedly for applying an external magnetic field of a few teslas [5], however, this superconductor is likely to be suitable to low-field applications so far. This means that the low-field applications are one of the key factors if the liquid hydrogen is used as a coolant of the MgB_2 wires. Hence, it is very promising that level sensors for the liquid hydrogen with the MgB_2 wires [6]–[9] become available in the near future.

In this paper, a superconducting induction/synchronous motor [10]–[15] for circulation or transfer of the liquid and/or slush hydrogen is presented as one of the low-field applications of the MgB_2 wires. This motor enables us to drive a pump to circulate or transfer the liquid/slush hydrogen with very low power consumption, and would form one of the infrastructure components in the near-future society with hydrogen utilization.

II. Proposal of Superconducting Motor for Liquid Hydrogen Pump

When the liquid hydrogen is transported with a pipeline or transfered at a hydrogen supply station in the near future, it is necessary to suppress the amount of heat generation during fluid transmission below an allowable level for the purpose that the liquid hydrogen as a high value-added fuel is vaporized as little as possible. The development of an electric pump for the liquid hydrogen with easy handling, compact size, and high performance has been desired, but such a liquid hydrogen pump has not been realized yet [16]–[19]. Up to now, a small liquid hydrogen transfer pump toward use at the hydrogen supply station has been designed, fabricated, and tested in the research and development projects of "the World Energy Network (WE-NET)" and the subsequent "Development for Safe Utilization and Infrastructure of Hydrogen" in Japan [20]. Although a squirrel-cage induction motor fabricated for driving the pump has been composed of rotor bars with aluminum, stator windings with copper wire, and iron cores with permalloy, the rotation test in the liquid hydrogen has resulted in the input power to the motor in a rated rotating speed twice as large as the design specification.

TABLE I Thermophysical Properties of Hydrogen [2]

Boiling temperature at 0.101 MPa	20.3 K
Saturation density of liquid phase at 0.101 MPa	70.8 kg/m^3
Saturation density of vapor phase at 0.101 MPa	1.34 kg/m^3
Mass density at 273 K and 0.101 MPa	0.0899 kg/m^3
Mass density at 273 K and 35 MPa	31 kg/m^3
Mass density at 273 K and 70 MPa	62 kg/m^3

Manuscript received 19 August 2008. This work was supported by the Industrial Technology Research Grant Program in 2008 (08B38006a) from the New Energy and Industrial Technology Development Organization (NEDO) of Japan.

K. Kajikawa is with the Research Institute of Superconductor Science and Systems, Kyushu University, Fukuoka 819-0395, Japan (corresponding author to provide phone: +81-92-802-3836; fax: +81-92-802-3829; e-mail: kajikawa@sc.kyushu-u.ac.jp).

T. Nakamura is with the Department of Electrical Engineering, Kyoto University, Kyoto 615-8510, Japan.

This means that the excessive load equal nearly to the pump power has been consumed somewhere.

Although the simple structure of the squirrel-cage induction motor provides cheap price and easy maintenance, the power consumption in the rotor winding becomes one of the major components of losses due to a slip phenomenon, which leads to a speed slower than a rotating magnetic field generated by the outer stator winding, indispensable to the torque output in principle. Therefore, the motors for the liquid hydrogen pump with superconducting wires are expected for drastic reduction of the power dissipation in the windings. So far, it has been confirmed experimentally [10], [12] that a synchronous rotating operation without slip in the squirrel-cage induction motor can be realized by replacing the rotor winding with high-temperature superconducting tapes. Additionally, a superconducting stator winding enables us to decrease the power consumption further as total system of the pump. Since both the windings for the rotor and stator in the motor are usually located in slots shaped into iron cores and the magnetic flux due to the transport currents almost passes through the iron cores, the superconducting wires are scarcely exposed to an external magnetic field and the self field becomes dominant. This means that the proposed superconducting motor for the liquid hydrogen pump is promising as one of the applications suitable to the present MgB_2 wires because the liquid hydrogen to be transfered itself acts as a coolant and the magnetic field applied to the windings are very small. Moreover, such a motor is immersed in the cryogenic liquid and the windings are cooled by it directly, so that it becomes unnecessary to consider a penalty factor of refrigeration [21], which has restricted the large-scale applications of superconductivity especially for AC use in comparison to the conventional techniques with the normal metal operated at room temperature.

The further advantages including the above-mentioned benefits in the proposed induction/synchronous motor for the liquid hydrogen pump are summarized as follows [12]–[15]:

1) Coexistence of slip and synchronous modes.
2) Low loss and high efficiency.
3) Large torque output.
4) Compact size and light weight.
5) Robust control for overload.
6) Self-field application of superconducting wires.
7) Freedom from penalty factor of refrigeration.

III. Outline Design of Rotor Winding

On the basis of the temperature dependence of transport properties observed in a MgB_2 wire with iron sheath [22], the outline design for an induction/synchronous motor with superconducting rotor winding is carried out in this section. It is assumed that the mono-cored MgB_2 wire with the outer diameter of 1.0 mm has a superconductor filament of 0.5 mm in diameter and a critical current of 150 A at the temperature of 20 K, as shown in Table II. The rotor bars consist of three strands of the MgB_2 wire, so that their critical current I_c becomes 450 A. Since the primary winding resistance, iron core loss, and mechanical loss at the liquid hydrogen temperature have not been estimated quantitatively and thus the optimum sharing between the electric and magnetic loadings required for motor design seems to be quite difficult, the operation properties of the induction/synchronous motor with the MgB_2 wire are predicted by referring to an commercially produced induction motor with the phase number m of three, the pole number p of four, and the rated output power of 1.5 kW as shown in Table III.

TABLE II Specifications of Magnesium-Diboride Wire [22]

Filament structure	Monofilament
Diameter of wire	1.0 mm
Diameter of superconductor filament	0.5 mm
Critical current at 20 K	150 A

TABLE III Specifications of Commercialized Induction Motor

Rated output power	1.5 kW
Number of phase	3
Number of pole	4
Rated voltage	200 V
Frequency	60 Hz
Turn number of primary winding	264 (delta connection)
Number of core slot for stator winding	36
Number of core slot for rotor winding	44
Primary resistance at room temperature	1.21 Ω
Total leakage inductance	9.63 mH
Synchronous rotating speed	1,800 rpm
Rated rotating speed	1,720 rpm
Rated torque	7.98 Nm

Table IV shows an example of the outline design of induction/synchronous motor with the MgB_2 wire. Based on the equivalent circuit analysis for the superconducting induction/synchronous motor [12]–[15], the maximum synchronous torque τ_{sm} is theoretically expressed by

$$\tau_{sm} = m\frac{p}{2}\Phi'_s I'_c, \tag{1}$$

where I'_c is the primary converted critical current of rotor bars estimated here as 16.9 A, and Φ'_s represents the primary converted trapped magnetic flux given by

$$\Phi'_s = \frac{\sqrt{V_1^2 - (\omega \ell' I'_c)^2} - r_1 I'_c}{\omega}, \tag{2}$$

where ω $(= 2\pi f)$ is the angular frequency for the frequency f of the input voltage V_1, ℓ' the primary converted total leakage inductance, and r_1 the primary resistance. Furthermore, the output power P_o at the synchronous rotating speed also becomes

$$P_o = \frac{2\omega}{p}\tau_{sm} = m\left\{\sqrt{V_1^2 - (\omega \ell' I'_c)^2} - r_1 I'_c\right\} I'_c. \tag{3}$$

It is assumed that the total leakage inductance ℓ' at the liquid hydrogen temperature is equal to that for the room temperature [13]–[15]. On the other hand, the primary winding resistance r_1 is obtained under the assumption that the residual resistance ratio (RRR), which is defined here by the ratio of the resistance at an operating temperature of the conventional motor to the resistance at 20 K, is a hundred for the copper.

TABLE IV OUTLINE DESIGN OF MOTOR WITH SUPERCONDUCTING ROTOR

Number of phase, m	3
Number of pole, p	4
Length of rotor core	88 mm
Outer diameter of rotor core	100 mm
Number of rotor core slot	44
Nominal voltage	200 V
Frequency, f	60 Hz
Operating temperature	20 K
Primary winding resistance, r_1	12.1 mΩ
Total leakage inductance, ℓ'	9.63 mH
Steady state rotating speed	1,800 rpm
Output power at synchronous mode, P_o	4.94 kW
Maximum synchronous torque, τ_{sm}	26.2 Nm

The skin effect for cyclic field due to very low resistivity of the normal metal at cryogenic temperature is not taken into account. In this case, the maximum synchronous torque τ_{sm} is estimated as 26.2 Nm, and the output power P_o becomes 4.94 kW. These results indicate that the superconducting rotor winding enables us not only to achieve the synchronous rotation without slip but also to improve the maximum torque and the output power more than three times larger than those for the conventional motor. The latter means that the superconducting machine becomes more compact for the requirement of output power or torque generation in given system.

IV. AC LOSS EVALUATION OF STATOR WINDING

In order to confirm the possibility of the further loss reduction by using superconducting wires for the stator winding in the motor, the numerical calculation is carried out on the basis of the conventional induction motor as shown in Table III again. The assumed MgB_2 wire is also identical with the previous section as already listed in Table II, except for electrical insulation on its surface. In this case, the required magnetomotive force is 234 A in peak value, so that it is assumed that the stator winding has three turns of the wire. This means that the rated primary current becomes 78 A in peak. Fig. 1 shows the cross-sectional view of the stator winding configuration in the conventional motor under consideration. The symbols, a, b, and c, represent the phase a, b, and c, respectively, and the sign means the direction of their current flow. Since one of the core slots has a couple of windings for different two phases, the net current given by the sum of their currents becomes equal to the other current in the opposite direction from the general relationship,

$$i_{\mathrm{a}} + i_{\mathrm{b}} + i_{\mathrm{c}} = 0, \tag{4}$$

for the three-phase alternating currents, i_{a}, i_{b}, and i_{c}, with phase difference of 120 degrees one another. The similar configuration for a superconducting stator is considered here for the numerical analysis.

If the magnetic permeability of iron core is infinite, the magnetic field strength inside the core becomes equal to zero and the magnetic flux lines just outside the core facing with the vacuum, which is magnetically equivalent to a region filled

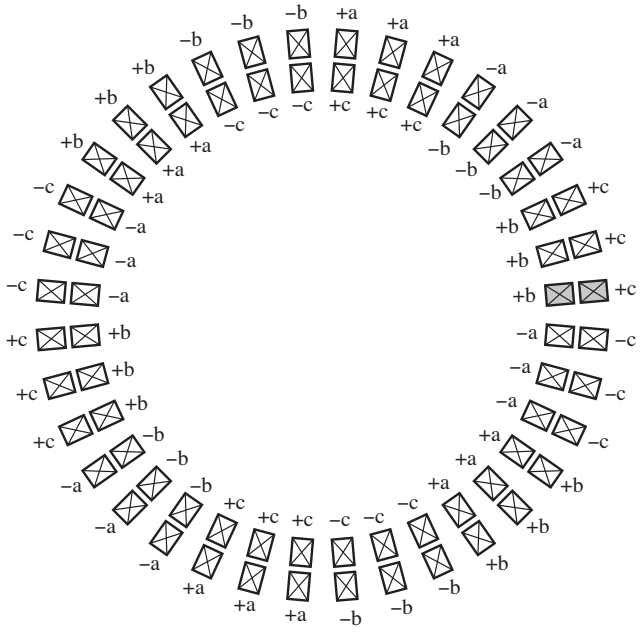

Fig. 1. Cross-sectional view of stator winding configuration with 3-phase, 4-pole, and 36 core slots. The shaded parts represent a couple of windings in a core slot focused on for numerical estimation of AC loss.

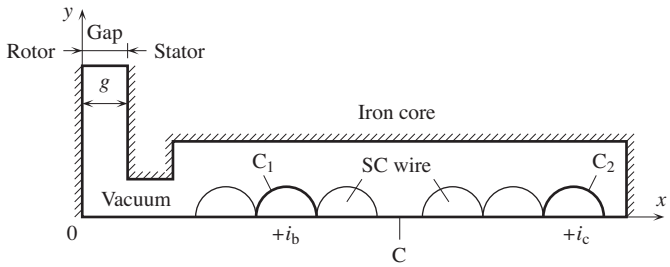

Fig. 2. Schematic diagram of half-size numerical model for core slot simplified to estimate AC loss in stator winding.

with the air or the cryogenic liquid, can be regarded as normal to the core surface. Moreover, it is enough to focus on only an isolated core slot for electromagnetic field analysis under the assumption that the entire magnetic flux due to the currents in the other windings passes through the core teeth and hence there is no flux in the core slot from the others. An example of the numerical model for core slot simplified to estimate the AC loss in the stator winding is shown in Fig. 2, where only a half part is taken into account because of its symmetric configuration. In this case, the governing equation formulated with a magnetic field $\boldsymbol{H}$ due to a current induced in the analysis region excluding the iron core is expressed by [23]

$$\nabla \times (\rho \nabla \times \boldsymbol{H}) = -\mu_0 \frac{\partial \boldsymbol{H}}{\partial t}, \tag{5}$$

where ρ is the resistivity. The boundary condition on the closed path C surrounding the entire analysis region is given by

$$\oint_{\mathrm{C}} \boldsymbol{H} \cdot \mathrm{d}\boldsymbol{s} = -H_g g = \frac{N i_{\mathrm{b}} + N i_{\mathrm{c}}}{2} = -\frac{N i_{\mathrm{a}}}{2},$$

$$\therefore H_g = \frac{N i_{\mathrm{a}}}{2g}, \tag{6}$$

TABLE V AC LOSS FOR STATOR WINDING WITH MAGNESIUM-DIBORIDE WIRE

Number of phase	3
Number of pole	4
Length of stator core	88 mm
Number of stator core slot	36
Frequency, f	60 Hz
Operating temperature	20 K
Magnetomotive force of primary winding	234 A_{peak}
Turn number of primary winding	3
Rated primary current	78 A_{peak}
AC loss in primary winding	0.45 W/phase
Corresponding primary resistance	0.15 mΩ/phase

where N is the turn number of winding, g the gap length between the iron cores for stator and rotor, H_g the magnetic field in the gap, and it is considered that the tangential components of magnetic fields on the surface of iron core and the symmetrical axis are equal to zero. The constrained condition on the path, C_1 or C_2, along every wire surface is also imposed as [24]

$$\oint_{C_1} \boldsymbol{H} \cdot \mathrm{d}\boldsymbol{s} = \frac{i_b}{2}, \qquad \oint_{C_2} \boldsymbol{H} \cdot \mathrm{d}\boldsymbol{s} = \frac{i_c}{2}. \tag{7}$$

Equation (5) is discretized with the Galerkin and backward difference methods for two-dimensional space and time, respectively, and the derived simultaneous equations are solved iteratively at each time step [23], [24]. By using the obtained distribution of magnetic field, the AC loss power P per unit length is numerically estimated with [23]

$$P = f \oint \mathrm{d}t \int_S \rho \, |\nabla \times \boldsymbol{H}|^2 \mathrm{d}S, \tag{8}$$

where S is the entire regions occupied by the superconductor.

An example of the numerical results of AC losses is given in Table V. The AC loss per phase is estimated as 0.45 W, and this corresponds to the primary resistance of 0.15 mΩ, which is much smaller than that for the copper wire in the cryogenic atmosphere, even if the RRR of the copper is a thousand.

V. CONCLUSION

The superconducting motors with the MgB_2 wires for circulation or transfer of the liquid/slush hydrogen were proposed and discussed in this study. The induction/synchronous motor composed of the MgB_2 rotor winding enables us to suppress the operation loss in the cryogenic environment due to the synchronous rotation mode and furthermore to reduce its volume and weight drastically as compared with the conventional induction motor. The use of MgB_2 stator winding also contributes not only to decrease the primary power consumption but also to realize the synchronous rotation mode in larger torque region. These prospective properties will be validated experimentally for fabricated MgB_2 induction/synchronous motors immersed in the liquid helium and surely in the liquid hydrogen in the near future.

REFERENCES

[1] H. Hirabayashi, "Liquid hydrogen and applied superconductivity—For advanced utilization in the community—," *TEION KOGAKU (J. Cryo. Soc. Jpn.)*, vol. 40, no. 7, pp. 276–283, July 2005.

[2] R. D. McCarty, "Hydrogen technology survey—Thermophysical properties," *NASA Special Publication*, SP-3089, Jan. 1975.

[3] K. Ohira, "Development of density and mass flow rate measurement technologies for slush hydrogen," *Cryogenics*, vol. 44, no. 1, pp. 59–68, Jan. 2004.

[4] J. Nagamatsu, N. Nakagawa, T. Muranaka, Y. Zenitani, and J. Akimitsu, "Superconductivity at 39 K in magnesium diboride," *Nature*, vol. 410, no. 6824, pp. 63–64, Mar. 2001.

[5] M. Tomsic, M. Rindfleisch, J. Yue, K. McFadden, D. Doll, J. Phillips, M. D. Sumption, M. Bhatia, S. Bohnenstiehl, and E. W. Collings, "Development of magnesium diboride (MgB_2) wires and magnets using in situ strand fabrication method," *Physica C*, vol. 456, nos. 1–2, pp. 203–208, June 2007.

[6] Ch. Haberstroh and G. Zick, "A superconductive MgB_2 level sensor for liquid hydrogen," *Adv. Cryo. Eng.*, vol. 51, pp. 679–684, May 2006.

[7] Ch. Haberstroh, G. Dehn, and D. Kirsten, "Liquid hydrogen level sensors based on MgB_2," *Proc. CryoPrague 2006*, no. 357, 2007.

[8] M. Takeda, Y. Matsuno, I. Kodama, and H. Kumakura, "Characteristics of MgB_2 sensor for detecting level of liquid hydrogen," *Adv. Cryo. Eng.*, vol. 53, pp. 933–939, Mar. 2008.

[9] K. Kajikawa, K. Tomachi, N. Maema, M. Matsuo, S. Sato, K. Funaki, H. Kumakura, K. Tanaka, M. Okada, K. Nakamichi, Y. Kihara, T. Kamiya, and I. Aoki, "Fundamental investigation of a superconducting level sensor for liquid hydrogen with MgB_2 wire," *J. Phys. Conf. Ser.*, vol. 97, 012140, Mar. 2008.

[10] J. Sim, M. Park, H. Lim, G. Cha, J. Ji, and J. Lee, "Test of an induction motor with HTS wire at end ring and bars," *IEEE Trans. Appl. Superconduct.*, vol. 13, no. 2, pp. 2231–2234, June 2003.

[11] J. Sim, K. Lee, G. Cha, and J.-K. Lee, "Development of a HTS squirrel cage induction motor with HTS rotor bars," *IEEE Trans. Appl. Superconduct.*, vol. 14, no. 2, pp. 916–919, June 2004.

[12] T. Nakamura, H. Miyake, Y. Ogama, G. Morita, I. Muta, and T. Hoshino, "Fabrication and characteristics of HTS induction motor by the use of Bi-2223/Ag squirrel-cage rotor," *IEEE Trans. Appl. Superconduct.*, vol. 16, no. 2, pp. 1469–1472, June 2006.

[13] G. Morita, T. Nakamura, and I. Muta, "Theoretical analysis of a YBCO squirrel-cage type induction motor based on an equivalent circuit," *Supercond. Sci. Technol.*, vol. 19, no. 6, pp. 473–478, June 2006.

[14] T. Nakamura, Y. Ogama, H. Miyake, K. Nagao, and T. Nishimura, "Novel rotating characteristics of a squirrel-cage-type HTS induction/synchronous motor," *Supercond. Sci. Technol.*, vol. 20, no. 10, pp. 911–918, Oct. 2007.

[15] T. Nakamura, K. Nagao, T. Nishimura, Y. Ogama, M. Kawamoto, T. Okazaki, N. Ayai, and H. Oyama, "The direct relationship between output power and current carrying capability of rotor bars in HTS induction/synchronous motor with the use of DI-BSCCO tapes," *Supercond. Sci. Technol.*, vol. 21, no. 8, 085006, Aug. 2008.

[16] H. Berndt, R. Doll, U. Jahn, and W. Wiedemann, "Low loss liquid helium transfer system, using a high performance centrifugal pump and cold gas exchange," *Adv. Cryo. Eng.*, vol. 33, pp. 1147–1152, 1988.

[17] H. Berndt, R. Doll, and W. Wiedemann, "Two years' experience in liquid helium transfer with a maintenance free centrifugal pump," *Adv. Cryo. Eng.*, vol. 35, pp. 1039–1043, 1990.

[18] G. Arnold and J. Wolf, "Liquid hydrogen for automotive application next generation fuel for FC and ICE vehicles," *TEION KOGAKU (J. Cryo. Soc. Jpn.)*, vol. 40, no. 6, pp. 221–230, June 2005.

[19] T. Aso, H. Tatsumoto, S. Hasegawa, I. Ushijima, K. Ohtsu, T. Kato, and Y. Ikeda, "Design result of the cryogenic hydrogen circulation system for 1 MW Pulse Spallation Neutron Source (JSNS) in J-PARC," *Adv. Cryo. Eng.*, vol. 51, pp. 763–770, May 2006.

[20] K. Kajikawa and T. Nakamura, "Proposal and outline design of fully superconducting motor for liquid hydrogen pump," *2008 Annual Meeting Record, I.E.E. Japan*, no. 5-110, Mar. 2008.

[21] I. Hlásnik, "Could a cryoturbogenerator armature winding be superconducting?," *Cryogenics*, vol. 23, no. 9, pp. 508–514, Sep. 1983.

[22] S. Balamurugan, T. Nakamura, K. Osamura, I. Muta, and T. Hoshino, "Annealing effects on structural and superconducting properties of MgB_2/Fe wires," *Mod. Phys. Lett. B*, vol. 18, no. 16, pp. 791–802, July 2004.

[23] K. Kajikawa, T. Hayashi, R. Yoshida, M. Iwakuma, and K. Funaki, "Numerical evaluation of AC losses in HTS wires with 2D FEM

formulated by self magnetic field," *IEEE Trans. Appl. Superconduct.*, vol. 13, no. 2, pp. 3630–3633, June 2003.

[24] T. Hayashi, K. Kajikawa, M. Iwakuma, and K. Funaki, "Numerical calculations of AC losses in parallel tape conductors with fixed share of transport current in external magnetic field," *Physica C*, vols. 426–431, part 2, pp. 1328–1332, Oct. 2005.